ELSEVIER

PII: S0032-3861(97)00423-0

Polymer Vol. 39 Nos. 6–7, pp. 1269–1278, 1998

0032-3861/97/$17.00+0.00

Dynamic mechanical and ^{13}C n.m.r. analyses of the effects of antiplasticization on the β secondary relaxation of aryl–aliphatic epoxy resins

L. Heux, F. Lauprêtre, J. L. Halary* and L. Monnerie
Laboratoire de Physicochimie Structurale et Macromoléculaire associé au CNRS, Ecole Supérieure de Physique et de Chimie Industrielles de la Ville de Paris, 10 rue Vauquelin, 75231 Paris Cedex 05, France
(Received 17 January 1997)

The antiplasticization of epoxy networks based on diglycidylether of bisphenol A (DGEBA) and hexamethylene diamine was investigated by both dynamic mechanical analysis and high-resolution solid-state ^{13}C nuclear magnetic resonance (n.m.r.) spectroscopy. Particular attention was paid to the influence of the antiplasticizer on the β secondary transition. In the case of densely crosslinked networks, the relevant loss peak of the antiplasticized material is dramatically reduced compared with that of the pure resin. The cooperative modes responsible for the high-temperature part of the β relaxation in the pure networks do not show up in the antiplasticized systems. N.m.r. measurements clearly demonstrate that the loss peak reduction is accompanied by a strong decrease in the mobility of the CH_2 groups that are close to the nitrogen crosslinks. In agreement with these observations, the efficiency of the antiplasticizer is weaker in the loosely crosslinked networks where the cooperative modes of the β transition are reduced. In the quasi-linear systems, where the β motions tend to be restricted to isolated motions, the efficiency of the antiplasticizer almost vanishes. This molecular description of the antiplasticization mechanism, in terms of hindrance of the short-scale cooperative motions in the glassy state, can be viewed as a dynamic coupling between the polymer and antiplasticizer molecule.

(Keywords: epoxy resins; antiplasticization; secondary relaxation)

INTRODUCTION

The motional processes that are responsible for the β secondary relaxation in epoxy resins have been studied extensively in a previous paper[1]. The assignment of the different parts of this broad transition was greatly facilitated by the use of different 'model' networks based on diglycidylether of bisphenol A (DGEBA) and either pure hexamethylene diamine (HMDA), or mixtures of HMDA with various amounts of hexylamine (HA) or dimethyl-hexamethylene diamine (DMHMDA). These systems have very much the same chain flexibility at the scale of the repeat unit. Their crosslink density is determined by the relative amount of HMDA with respect to the other amine (HA or DMHMDA). In addition, it is worth noticing that HA- and DMHMDA-based systems exhibit a different architecture. Networks prepared in the presence of HA primary monoamine have pendant hexamethylene units, whereas the role of the DMHMDA secondary diamine is to extend the mesh of the networks by inserting flexible units in the chains containing the bisphenol A residue.

In agreement with results obtained by Shi *et al.*[2], the high-resolution solid-state ^{13}C nuclear magnetic resonance (n.m.r.) experiments reported in [1] indicated that the motions of the hydroxypropylether units take part in the β transition, together with the DGEBA ring flips. Moreover, in these systems, the extent of the β transition depends strongly on the crosslink density. As shown by dynamic mechanical analysis, in a densely crosslinked network, localized motions at the spatial scale of an epoxy–amine repeat unit occur at low temperatures, whereas cooperative modes implying more than six units are responsible for the high-temperature part of the relaxation. In the quasi-linear systems, only modes with a low spatial extent exist. In contrast with networks incorporating pendant hexamethylene units, networks prepared by using secondary diamines exhibit a higher intramolecular cooperativity.

Another way of probing the motional processes that are involved in the β relaxation of epoxy resins is to study the modifications that accompany the introduction of an additive, either a plasticizer or an antiplasticizer. Antiplasticization is defined by an increase of the stress at the yield point, an increase of the tensile modulus at room temperature and a decrease of the elongation at break[3]. In epoxy resins, it also induces a strong reduction of the β transition[4–6]. It must be noticed that the mechanism of antiplasticization in epoxy resins is not yet fully understood; whereas, in antiplasticized polycarbonate, antiplasticization is clearly related to changes in the sub-T_g (glass transition temperature) local dynamics of the polymer[7–9], it has been described in terms of changes in the supramolecular structure[10,11] or densification in epoxy systems[4–6,12].

In the present paper, we shall analyse the β relaxation of epoxy systems antiplasticized by the additive developed by Garton *et al.*[6], by using both the model networks and the combination of dynamic mechanical analysis and

* To whom correspondence should be addressed

high-resolution solid-state ^{13}C n.m.r. that proved most useful in our previous study of the pure materials[1]. There are two aims for our work: the first is to obtain a better insight into the phenomena associated with the β relaxation, the second is to reach a deeper understanding of the mechanism of antiplasticization in epoxy resins.

EXPERIMENTAL

Materials

The characteristics and origins of the chemicals used in this study are given in *Table 1*.

The antiplasticizer EPPHAA was synthesized by following the procedure described by Daly *et al.*[6]. Epoxyphenoxypropane (EPP) and hydroxyacetanilide (HAA) at a 1.05:1 molar ratio were mixed and heated to 160°C for 1 h in the presence of 0.1 wt% diethylamine hydrochloride (Acros Organics) as catalyst. EPPHAA was obtained in the form of a yellow amorphous material and was used without further purification. Its glass transition temperature is 30°C, as determined by differential scanning calorimetry (d.s.c.) at a heating rate of 10°C min^{-1}.

EPPHAA was added to the diepoxide and heated at 60°C with stirring. After a homogeneous mixture was obtained, quick degassing was performed under vacuum. ^{13}C n.m.r. spectra in solution have shown that no epoxy ring opening occurs during this step, indicating the absence of a chemical reaction between DGEBA and EPPHAA under these conditions. Then, stoichiometric proportions of HMDA (or of mixtures of HMDA and HA or of HMDA and DMHMDA, depending of the type of network to be prepared) were added and the mixtures were kept under stirring until homogeneity. Finally, the samples were cured under a nitrogen atmosphere, first at 40°C for 12 h, and then at 30°C above the T_g of the pure network for 24 h[1].

Characterization of the EPPHAA-antiplasticized systems

The code names and compositions of the different samples under study are listed in *Table 2*.

Kinetic studies were performed following procedures described in another paper[13]. They demonstrated that the

Table 1 Characteristics and origins of the chemicals used in this study

Chemical	Formula	Origin
diglycidylether of bisphenol-A (DGEBA)	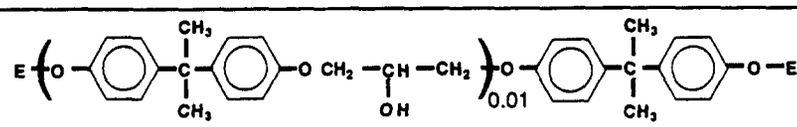 with E = 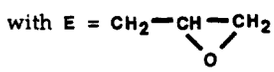	Bakelite (Rutapox 162
hexamethylenediamine (HMDA)	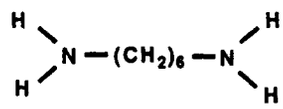	Aldrich
hexylamine (HA)	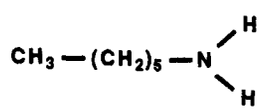	Merck
N,N dimethyl hexamethylenediamine (DMHMDA)	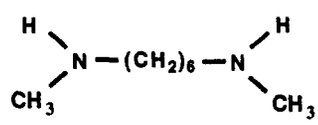	Aldrich
epoxyphenoxypropane (EPP)	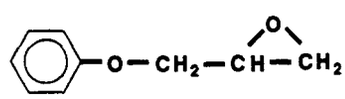	Aldrich
hydroxyacetanilide (HAA)	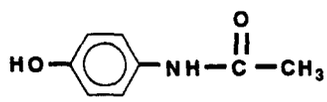	Aldrich
EPPHAA	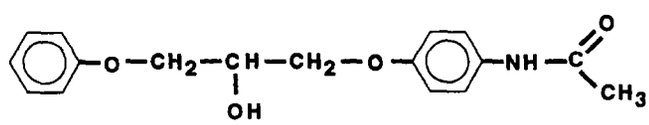	Our laboratory

Table 2 Code names, compositions and glass transition temperatures of the samples

Code name	Epoxy moiety	Amine moiety	EPPHAA (wt%)	T_g (°C)
HMDA	DGEBA	HMDA	0	121
HMDA/AP10	DGEBA	HMDA	10	80
HMDA/AP19	DGEBA	HMDA	19	68
HA60[a]	DGEBA	25 mol% HMDA, 75 mol% HA	0	70
HA60/AP19	DGEBA	25 mol% HMDA, 75 mol% HA	19	45
HA95[a]	DGEBA	2.5 mol% HMDA, 97.5 mol% HA	0	56
HA95/AP19	DGEBA	2.5 mol% HMDA, 97.5 mol% HA	19	39
DMHMDA60[a]	DGEBA	25 mol% HMDA, 75 mol% DMHMDA	0	60
DMHMDA60/AP19	DGEBA	25 mol% HMDA, 75 mol% DMHMDA	19	33
DMHMDA95[a]	DGEBA	2.5 mol% HMDA, 97.5 mol% DMHMDA	0	32
DMHMDA95/AP19	DGEBA	2.5 mol% HMDA, 97.5 mol% DMHMDA	19	28

[a]60 and 95 refer to the percentages of NH groups belonging to the difunctional amine moiety in the reactive mixture

reaction rate is substantially increased in the presence of EPPHAA, probably as the result of the catalytic effect of the OH functions present in the additive. However, the overall extent of reaction after post-cure is the same, within experimental accuracy (about 5%), in pure and antiplasticized networks. This conclusion holds whatever the architecture (densely crosslinked, loosely crosslinked or quasi-linear) of the system under consideration. Therefore, the presence of EPPHAA in the mixture of reactive monomers does not modify the chemical structure of the networks.

The d.s.c. traces of all the antiplasticized samples exhibit a single well-defined glass transition at a temperature which is intermediate between the EPPHAA glass transition temperature and the glass transition temperature of the pure network. This single glass transition temperature depends on the amount of EPPHAA in the system. These results indicate that the antiplasticizer and epoxy networks are miscible.

Densities were measured at 23°C by following the procedure described elsewhere for the pure systems[14].

Dynamic mechanical analysis

Viscoelastic experiments were performed at very low deformation (0.1%) by using the equipments and methods described in our previous paper[1]. The HA95/AP19 sample was too brittle to be subjected to dynamic mechanical analysis.

Data analysis was based on: (1) the storage modulus, E', for stiffness comparison, (2) the loss modulus, E'', for master curve construction and activation enthalpy and entropy calculations, and (3) the loss compliance, J'' [$= E''/(E'^2 + E''^2)$], for a semi-quantitative comparison of the mechanical damping of the different systems.

The glass transition temperatures of the networks were conventionally taken at the maximum of E'' at the frequency of 1 Hz. They are given in *Table 2*.

In the β transition range, master curves were constructed according to shifts, a_{T/T_0}, along the reciprocal temperature axis. The activation energy, E_a, was calculated by assuming an Arrhenius dependence of the shift factors:

$$\ln a_{T/T_0} = \frac{E_a}{R}\left(\frac{1}{T} - \frac{1}{T_0}\right)$$

The activation enthalpy, $\Delta H^{\ddagger}$, and entropy, $\Delta S^{\ddagger}$, were derived from the relationships proposed by Starkweather[15]:

$$\Delta H^{\ddagger} = E_a - RT_0 \quad \text{and} \quad \Delta S^{\ddagger} = E_a - RT_0\left[1 + \ln\left(kT_0/2\pi h\right)\right]$$

where R, k and h are the gas constant, Boltzmann's constant and Planck's constant, respectively, and T_0 is the characteristic temperature relative to the reference frequency of 1 Hz.

In our analysis, the β transition peak was divided into three parts: (1) the low-temperature range ($E'' < E_{max}''/3$, $T < T_{max}$), characterized by $E_{a_{beg}}$, $\Delta H^{\ddagger}_{beg}$ and $\Delta S^{\ddagger}_{beg}$; (2) the middle temperature range around the maximum ($E'' \approx E_{max}''$, $T \approx T_{max}$), characterized by $E_{a_{mid}}$, $\Delta H^{\ddagger}_{mid}$ and $\Delta S^{\ddagger}_{mid}$; and (3) the high-temperature range ($E'' < E_{max}''/3$, $T > T_{max}$), characterized by $E_{a_{end}}$, $\Delta H^{\ddagger}_{end}$ and $\Delta S^{\ddagger}_{end}$.

N.m.r. measurements

The 75 MHz ^{13}C n.m.r. spectra were obtained on a Bruker ASX300 spectrometer using the combined techniques of proton dipolar decoupling, magic-angle sample spinning and cross-polarization[16]. ^{13}C and ^{1}H magnetic field strengths of 64 kHz were used for the matched spin-lock cross-polarization transfer. The spinning speed was of the order of 4 kHz.

Inversion recovery cross-polarization (ICRP) experiments were made by using the pulse sequence proposed by Cory[17]. The phase of the proton channel was inverted after a 1 ms contact time. Experiments were performed as a function of the duration of the second contact time.

The $t_{1/2}$ values were determined at 75 MHz from the dependence of the intensities of the different CH or CH_2 lines as a function of the contact time in cross-polarization experiments with very short contact times, as described in [1]. The maximum magnetization that can be acquired by cross-polarization, S_{max}, was derived by extrapolating, to zero time, the $T_{1\rho}(^1H)$ decrease of the ^{13}C magnetization observed at long contact times. The accuracy for a $t_{1/2}$ determination is of the order of 0.5 μs.

^{13}C spin–lattice relaxation times in the rotating frame, $T_{1\rho}(^{13}C)$, were measured by using the carbon spin-locking sequence described in [18] and recording the ^{13}C magnetization decay as a function of the variable time, Δt, during which the carbons are held in their rotating frame without cross-polarization contact with the protons. The Δt values used for the $T_{1\rho}(^{13}C)$ determinations ranged from 50 μs to 500 μs, as proposed by Schaefer *et al.*[18].

The principal values of the chemical shift anisotropy tensor were derived from the relative intensities of the spinning side bands, by means of Herzfeld and Berger calculations[19].

RESULTS AND DISCUSSION

The densities of pure[14] and antiplasticized networks are listed in *Table 3*. The density, ρ_M, of any antiplasticized

Table 3 Densities of the pure and antiplasticized systems

Network	ρ_M (g cm^{-3})	ρ_N^a (g cm^{-3})	ρ_C (g cm^{-3})	$\Delta\rho$ (g cm^{-3})
HMDA	1.184	1.163	1.173	0.011
HA60	1.160	1.141	1.155	0.005
DMHMDA60	1.148	1.135	1.150	− 0.002
HA95	1.139	1.123	1.140	− 0.001

[a]Data taken from [14]

Table 4 C_1^g, C_2^g, f_g and α_f values in pure and antiplasticized networks

Network	C_1^g	C_2^g (°C)	$10^2 \times f_g/B$	$10^3 \times \alpha_f/B$
HMDA[a]	11.0	42	3.95	0.94
HMDA/AP10	12.0	41	3.62	0.88
HMDA/AP19	12.9	42	3.37	0.80
HA60[a]	9.9	34	4.39	1.29
HA60/AP19	11.9	38	3.65	0.96
DMHMDA60	7.9	22	5.50	2.50
DMHMDA60/AP19	10.2	25	4.26	1.71

[a]Data taken from [21]

system is systematically higher than the density of its pure homologue, ρ_N. This increase in density is consistent with earlier observations on densely crosslinked epoxy matrices[4–6]. However, since the measured density, ρ_A, of EPPHAA (1.217 g cm^{-3}) is larger than the density, ρ_N, of any pure epoxy resin, densification effects are reflected by the relevant quantity:

$$\Delta\rho = \rho_M - \rho_C = \rho_M - \frac{1}{[w_A/\rho_A] + [(1-w_A)/\rho_N]}$$

where w_A is the additive weight fraction. As can be seen in *Table 3*, $\Delta\rho$ is negligible in the quasi-linear HA95/AP19 system and in the mesh extender, loosely crosslinked DMHMDA60/AP19 network. In contrast, densification is observed in the loosely crosslinked network HA60/AP19 and is quite significant in the densely crosslinked HMDA/AP19 network.

Information on the dynamic free volume characteristics of the samples was deduced from the analysis of the viscoelastic data above T_g. According to the frequency–temperature superposition principle[20], the different curves E' (or E'') *versus* frequency may be reduced to a unique master curve, provided appropriate shifts, $\log a_T$, are made along the frequency scale. By fitting the temperature dependence of $\log a_T$ in the T_g region by the well-known WLF equation:

$$\log a_T = \frac{-C_1^g(T-T_g)}{C_2^g + T - T_g}$$

the values of the viscoelastic coefficients C_1^g and C_2^g at the reference temperature T_g were derived from the plot of $(T_g - T)/\log a_T$ *versus* $(T - T_g)$. C_1^g and C_2^g are related to the fractional free volume available at T_g, f_g, and the expansion coefficient of the free volume above T_g, α_f:

$$C_1^g = \frac{B}{2.3 f_g}$$

$$C_2^g = \frac{f_g}{\alpha_f}$$

and thus

$$C_1^g \cdot C_2^g = \frac{B}{2.3\alpha_f}$$

where B is usually taken equal to unity. As shown in *Table 4*, decreases of both f_g and α_f are observed in the HMDA/AP10 and HMDA/AP19 networks: the larger the amount of EPPHAA, the greater the decreases of f_g and α_f. The decrease in free volume characteristics seems to hold irrespective of network architecture. Therefore, these results show that the addition of the miscible EPPHAA additive induces some reduction in the dynamic free volume in the sample.

Viscoelastic response of the antiplasticized networks in the glassy state

Densely crosslinked DGEBA–HMDA networks. Figure 1a shows the temperature dependence of the loss compliance, J'', determined at 1 Hz, for the HMDA, HMDA/AP10 and HMDA/AP19 samples. It is clear that the three samples exhibit the same behaviour in the low-temperature part of the β secondary relaxation. In contrast, the high-temperature component of the β peak is progressively suppressed in the presence of increasing amounts of antiplasticizer. These observations are consistent with earlier studies of Hata *et al.* on DGEBA–ethylene diamine networks[4–6] and Garton *et al.* on DGEBA–diaminodiphenylmethane networks[12].

In order to perform a semi-quantitative evaluation of the antiplasticization effects on the β transition, the $J_{HMDA}'' - J_{HMDA/AP10}''$ and $J_{HMDA}'' - J_{HMDA/AP19}''$ differences are compared with the loss compliance of the pure network in *Figure 1b*. Such difference plots are representative of the part of the relaxation that has been suppressed under the action of the antiplasticizer. Three main features are apparent from *Figure 1b*: (1) the antiplasticizer has no effect on the low-temperature mechanically active motions, (2) the antiplasticizer hinders all the high-temperature motions, whatever its amount (10 or 19 wt%), and (3) the efficiency of the antiplasticizer in the intermediate temperature range increases with its concentration in the network. According to our previous conclusions on the degree of cooperativity of the β motions as a function of temperature[1], these results would imply that the capability of the antiplasticizer to hinder local motions is strong when dealing with cooperative processes. It decreases when the spatial scale of cooperativity decreases and finally vanishes when isolated motions only are occurring.

This conclusion is supported by measurements performed

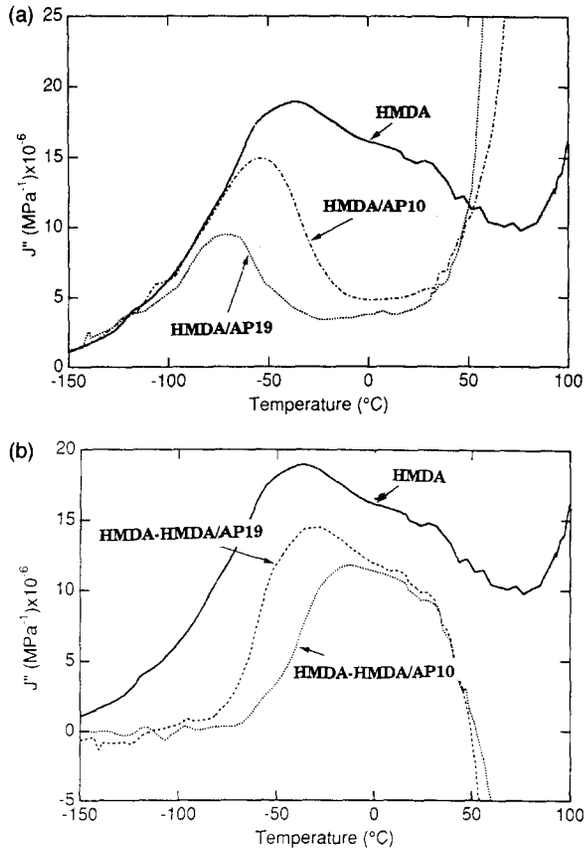

Figure 1 (a) Temperature dependence of the loss compliance, J'', determined at 1 Hz for the HMDA, HMDA/AP10 and HMDA/AP19 systems; (b) temperature dependences of J_{HMDA}'' and the differences $J_{HMDA}'' - J_{HMDA/AP10}''$ and $J_{HMDA}'' - J_{HMDA/AP19}''$

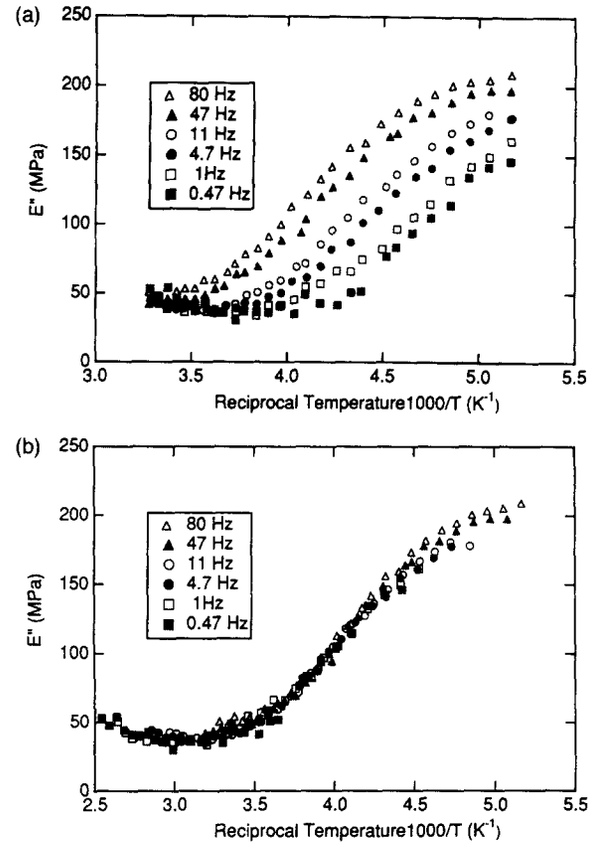

Figure 2 (a) Dependence of E'' as a function of frequency and reciprocal temperature in the HMDA/AP19 system; (b) master curve construction according to the frequency–temperature superposition principle

at various frequencies. As shown in [1], the impossibility of drawing a consistent master curve all over the β transition E'' peak is indicative of the existence of different types of motion; on the other hand, successful building of a master curve is regarded as evidence for a simple motional behaviour on the whole temperature range corresponding to the β transition. The former situation is encountered in the pure HMDA network[1]. The latter situation is observed for the HMDA/AP19 system (*Figure 2a* and *Figure 2b*), where most of the cooperative motions are hindered by the presence of EPPHAA.

E_a, $\Delta H^{\ddagger}$ and $\Delta S^{\ddagger}$ values derived from the Starkweather analysis[15] at the beginning, middle part and end of the β transition for the HMDA, HMDA/AP10 and HMDA/AP19 networks are listed in *Table 5*. The $\Delta S^{\ddagger}$ values can be considered as an indication of motional cooperativity. Values of the order of 100 J K^{-1} mol^{-1} or larger are observed in the central and high-temperature parts of the E'' peak of the pure network. They correspond to a rather high motional cooperativity. On the other hand, very small $\Delta S^{\ddagger}$ values (30 J K^{-1} mol^{-1} or less for HMDA/AP19) are observed in the antiplasticized systems. They account for the hindrance of most of the cooperative motions. As expected, in the high-temperature part of the transitions, $\Delta S^{\ddagger}$ is larger for HMDA/AP10 than for HMDA/AP19 since the antiplasticization effect is somewhat weaker.

The room-temperature modulus fortifier effect of the antiplasticizer EPPHAA is clearly demonstrated by the values of the storage modulus, E', at 1 Hz. As shown in *Figure 3*, E' has very similar values for the HMDA, HMDA/AP10 and HMDA/AP19 samples at the onset of the transition, i.e. around − 150°C. By contrast, the E' value at room temperature increases on increasing the amount of EPPHAA. E' is multiplied by a factor of two when going from the pure network to the network prepared in the presence of 19 wt% additive. The comparison of low-temperature and room-temperature data clearly shows that the modulus fortifier effect at room temperature results from a lower decrease of E' along the β transition region in the antiplasticized samples. The E' and E'' viscoelastic quantities are not independent of each other, since they are the real and imaginary components of the complex modulus E^*; therefore, the larger the mechanical energy loss in the E'' peak, the stronger the decrease of E'. Thus, the modulus fortifier effect is simply the consequence of the reduction of the E'' peak width and amplitude in the presence of the antiplasticizer.

Quasi-linear HA95 and loosely crosslinked HA60 systems

. The introduction of monoamine in the resin formulation induces a decrease of the crosslink density, associated with the presence of pendant groups. J'' data plotted in *Figure 4* exhibit a narrowing and reduction in amplitude of the β peak in the quasi-linear HA95 system. This result has been interpreted in terms of an absence of high-temperature cooperative motions[1]. Since, in the HMDA network, the antiplasticizer has been shown to affect the cooperative motions only, the influence of EPPHAA on the HA95 system should be weak. This result is indeed observed in *Figure 4a*. With respect to data obtained on the pure HA95 sample, the shape of the J'' peak is nearly unchanged in the HA95/AP19 resin and its amplitude is only slightly reduced. The difference spectrum ($J_{HA95}'' - J_{HA95/AP19}''$) shows that

Table 5 Characteristic temperatures (T), and activation energies (E_a), enthalpies ($\Delta H^{\ddagger}$) and entropies ($\Delta S^{\ddagger}$), in the β relaxation region for the different systems under study. Data relative to the pure systems are taken from [1]

	T beginning (K)	E_a beginning (kJ mol^{-1})	T maximum (K)	E_a maximum (kJ mol^{-1})	T end of peak (K)	E_a end of peak (kJ mol^{-1})
HMDA	150	36	212	70	277	111
HMDA/AP10	150	37	209	60	235	71
HMDA/AP19	150	34	196	51	226	60
HA60	145	34	199	53	234	80
HA60/AP19	150	37	196	51	225	61
HA95	140	32	190	50	218	64
HA95/AP19	140	35	190	45	216	58
DMHMDA60	145	34	205	72	240	85
DMHMDA60/AP19	145	39	199	65	234	82
DMHMDA95	145	35	199	64	235	85
DMHMDA95/AP19	145	38	196	59	230	82
	$\Delta H^{\ddagger}$ beginning (kJ mol^{-1})	$\Delta S^{\ddagger}$ beginning (J mol^{-1} K^{-1})	$\Delta H^{\ddagger}$ maximum (kJ mol^{-1})	$\Delta S^{\ddagger}$ maximum (J mol^{-1} K^{-1})	$\Delta H^{\ddagger}$ end of peak (kJ mol^{-1})	$\Delta S^{\ddagger}$ end of peak (J mol^{-1} K^{-1})
HMDA	35	7	68	95	108	163
HMDA/AP10	36	14	58	52	69	66
HMDA/AP19	33	0	49	26	58	30
HA60	33	3	51	31	78	105
HA60/AP19	35	7	40	26	59	36
HA95	31	0	48	28	62	58
HA95/AP19	33	11	45	13	59	33
DMHMDA60	33	9	70	116	83	118
DMHMDA60/AP19	38	37	63	92	82	114
DMHMDA95	34	3	62	87	83	125
DMHMDA95/AP19	36	30	57	66	80	121

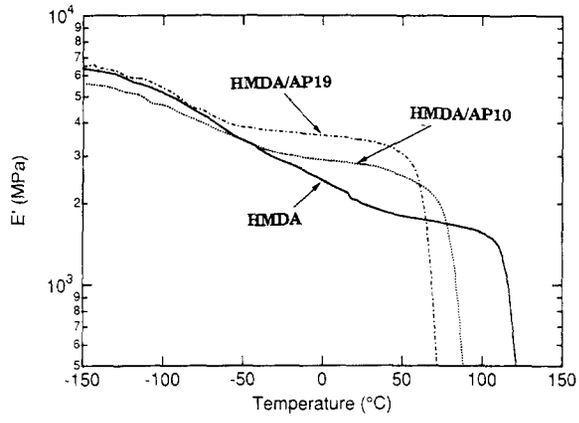

Figure 3 Temperature dependence of the storage modulus, E', determined at 1 Hz for the HMDA, HMDA/AP10 and HMDA/AP19 systems

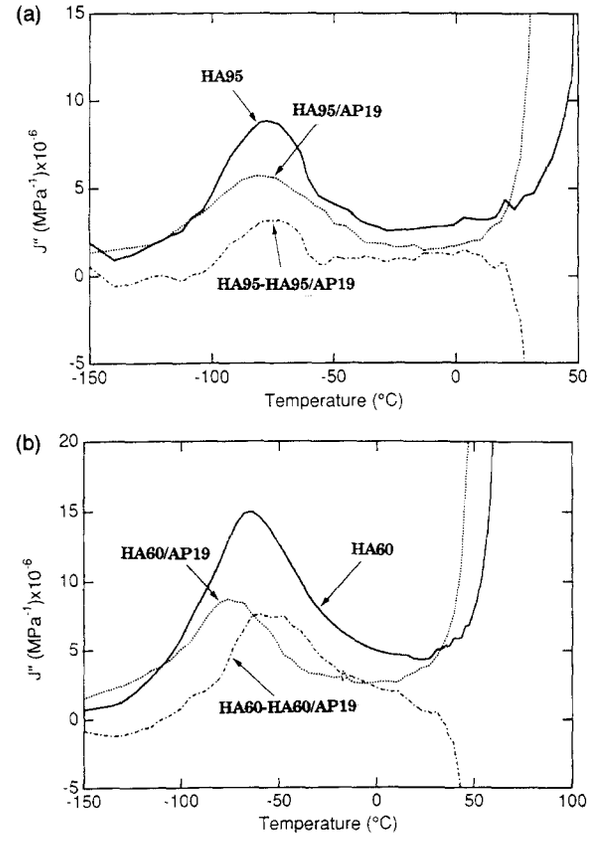

Figure 4 Temperature dependences of J_{HA95}'', $J_{HA95/AP19}''$ and $J_{HA95}'' - J_{HA95/AP19}''$ (a) and of J_{HA60}'', $J_{HA60/AP19}''$ and $J_{HA60}'' - J_{HA60/AP19}''$ (b)

only the highest temperature modes are modified. In agreement with this interpretation, it can be noticed that consistent master curves of E'' *versus* reciprocal temperature can be plotted and that the Starkweather analysis of the activation energy leads to very low values of $\Delta S^{\ddagger}$ (*Table 5*). In the HA60/AP19 system (*Figure 4b*), the effect of the antiplasticizer is intermediate between the behaviours observed in the densely crosslinked network and quasi-linear system, because some residual cooperative motions are still available in the pure network and can be hindered by the presence of the antiplasticizer.

Quasi-linear DMHMDA95 and loosely crosslinked DMHMDA60 systems. The introduction of secondary

diamine in the resin formulation also leads to a decrease of the crosslink density. However, as regards the β secondary transition, the mesh extender architecture allows intramolecular cooperative motions to develop, even in the quasi-linear DMHMDA95 system[1]. Therefore, the question addressed in the present section is to determine whether the antiplasticizer prevents these intramolecular cooperative motions from occurring.

The loss compliances J'' of the DMHMDA95 and DMHMDA95/AP19 systems are plotted in *Figure 5a*. The β peak amplitude is reduced in the DMHMDA95/AP19 sample. Analysis of the difference ($J_{DMHMDA95}'' - J_{DMHMDA95/AP19}''$) indicates that some high-temperature motions are unambiguously hindered. However, compared with the data reported in *Figure 2a*, the efficiency of the additive is rather poor. In the DMHMDA60/AP19 network, the influence of the antiplasticizer is clearly seen in the high-temperature range (*Figure 5b*). However, its role cannot be precisely described since both inter- and intramolecular cooperative motions are likely to occur in the pure homologue.

E'' measurements performed at various frequencies on the DMHMDA95/AP19 sample are shown in *Figure 6a*. As for DMHMDA95[1], a consistent master curve cannot be derived from these data in the high-temperature range of the β transition (*Figure 6b*, see *Figure 2b* for comparison). In agreement with the analysis of the compliance plots, this result reveals the lack of efficiency of EPPHAA in this sample. This conclusion is also supported by the $\Delta S^{\ddagger}$ values calculated in these systems (*Table 5*): the entropic contribution to the β process is quite similar for pure and antiplasticized DMHDA-based networks.

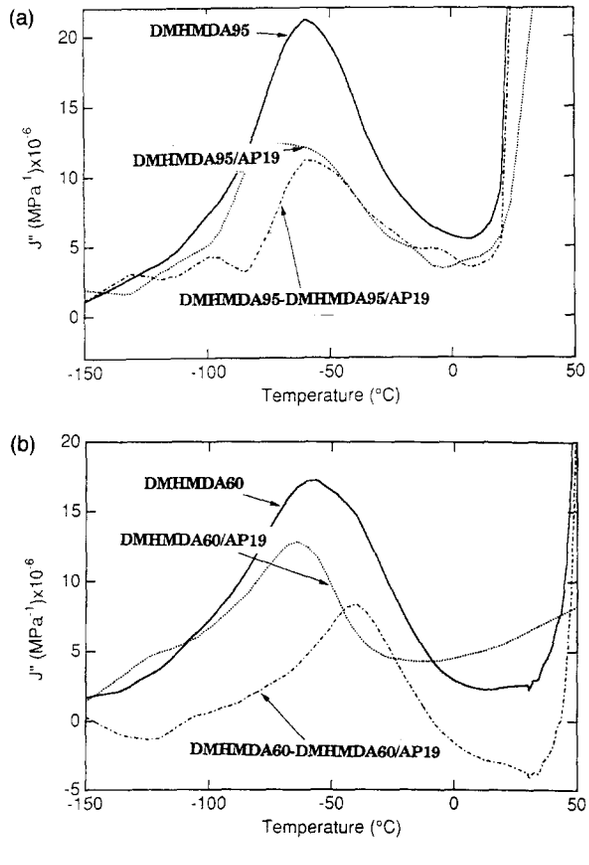

Figure 5 Temperature dependences of $J_{DMHMDA95}''$, $J_{DMHMDA95/AP19}''$ and $J_{DMHMDA95}'' - J_{DMHMDA95/AP19}''$ (a) and of $J_{DMHMDA60}''$, $J_{DMHMDA60/AP19}''$ and $J_{DMHMDA60}'' - J_{DMHMDA60/AP19}''$ (b)

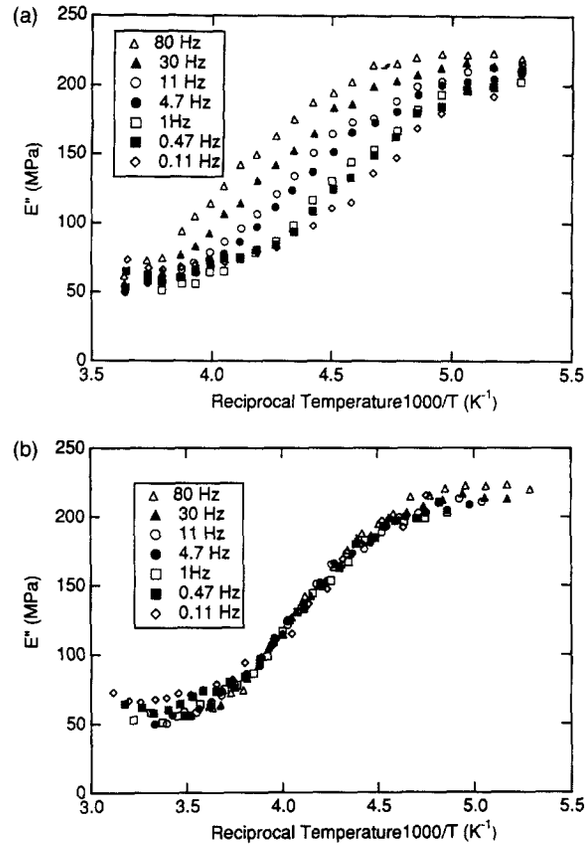

Figure 6 (a) Dependence of E'' on frequency and reciprocal temperature in the DMHMDA95/AP19 system; (b) attempt at master curve construction with the frequency–temperature superposition principle

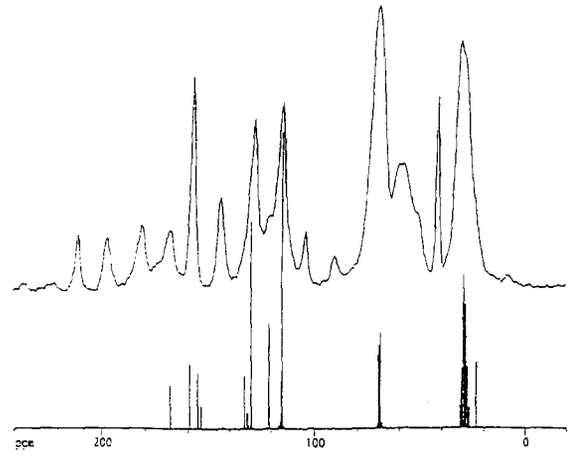

Figure 7 Top spectrum: 75 MHz high-resolution solid-state ^{13}C n.m.r. spectrum of the HMDA/AP19 network at 30°C (contact time = 1 ms). Bottom spectrum: 25 MHz ^{13}C n.m.r. spectrum of the EPPHAA antiplasticizer in CD_3COCD_3 solution

N.m.r. investigation of local motions in the HMDA/AP19 network

Figure 7 displays the 75 MHz high-resolution solid-state ^{13}C n.m.r. spectrum of the HMDA/AP19 network. The assignment of the lines of the matrix has been described elsewhere[1,22]. In order to characterize the contribution of the antiplasticizer, the 25 MHz ^{13}C n.m.r. spectrum of EPPHAA in CD_3COCD_3 solution is also shown. Because of the similarities in their chemical structure, the lines arising from the $CHOH-CH_2-O$ sequences of the polymer matrix and antiplasticizer overlap. The chemical shifts of

the aromatic lines of the epoxy network and EPPHAA molecule are very similar. The resonance of the EPPHAA carbonyl carbon coincides with a spinning sideband of a DGEBA aromatic carbon resonance. The line of the EPPHAA methyl carbon is hidden by the peaks of the central CH_2 carbons of the diamine unit.

Local motions of the aliphatic units. The investigation of the local dynamics is based on measurements of the $^1H-^{13}C$ dipolar couplings[1,23] and ^{13}C spin–lattice relaxation times in the rotating frame.

The $t_{1/2}$ values, determined for the CHOH–CH_2–O and CH_2–N carbons of the hydroxypropylether sequence at room temperature, are equal to 22.5 μs and 19.5 μs, respectively, in the HMDA, HMDA/AP10 and HMDA/AP19 systems. These $t_{1/2}$ values are the rigid-lattice values, $(t_{1/2})_0$, for these groups. The temperature dependence of the $(t_{1/2})_0/t_{1/2}$ ratio, measured for the CHOH–CH_2–O and CH_2–N carbons in the HMDA, HMDA/AP10 and HMDA/AP19 systems, is displayed in *Figure 8a* and *Figure 8b*. Over the temperature range investigated, the behaviour of the $(t_{1/2})_0/t_{1/2}$ ratio of the CH_2–N units is significantly different in the three samples. In contrast with results observed for the pure resin, the $(t_{1/2})_0/t_{1/2}$ ratio of the CH_2–N units of the HMDA/AP19 system does not depend on temperature, which indicates the absence of motions with frequency higher than 10^5 Hz at temperatures up to 90°C. In the HMDA/AP10 resin, the $(t_{1/2})_0/t_{1/2}$ ratio, which is equal to 0.9 at 100°C, has a very weak temperature dependence. Therefore, the motions of the CH_2 group next to the crosslinks are strongly restricted in the HMDA/AP10 network and totally hindered in the HMDA/AP19 system. The difference in the behaviour

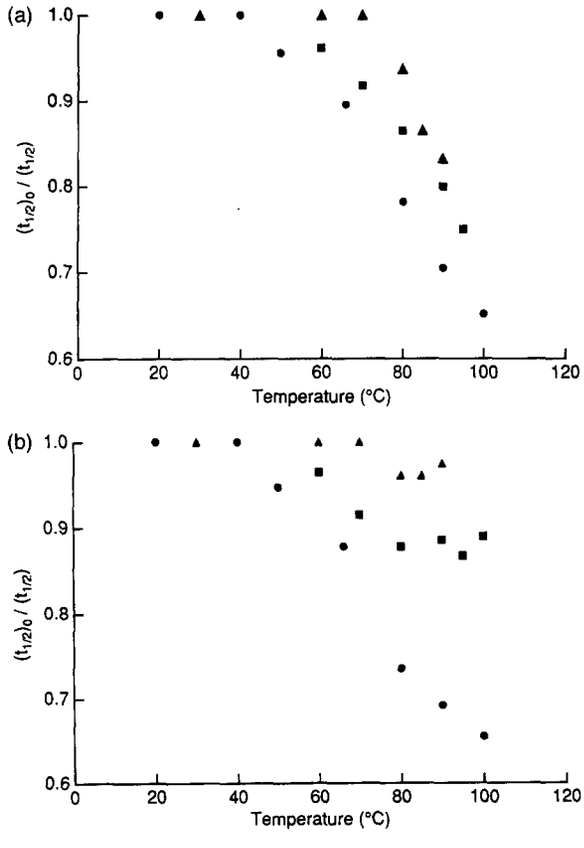

Figure 8 Temperature dependence of the $(t_{1/2})_0/t_{1/2}$ ratios in HMDA (●), HMDA/AP10 (■) and HMDA/AP19 (▲) networks: (a) CHOH–CH_2–O carbons; (b) CH_2–N carbons

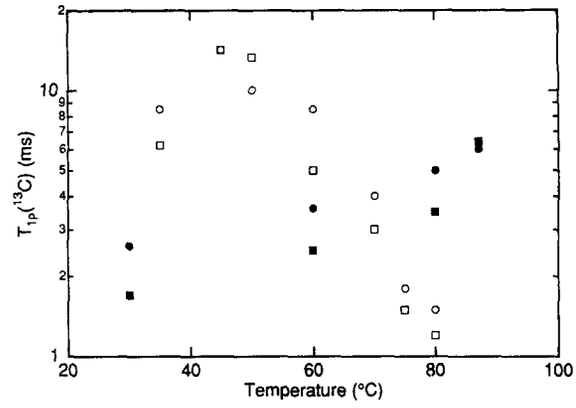

Figure 9 Temperature dependence of the ^{13}C spin–lattice relaxation times in the rotating frame for the HMDA (●, CHOH–CH_2–O carbons; ■, CH_2–N carbons) and HMDA/AP19 (○, CHOH–CH_2–O carbons; □, CH_2–N carbons) networks

of the CHOH–CH_2–O sequence in the pure and antiplasticized networks is less pronounced. When the antiplasticizer content increases, a small increase in the temperature at which the onset of mobility is observed, showing that the presence of the antiplasticizer induces a slight slowing down of the CHOH–CH_2–O motions.

The temperature dependence of the ^{13}C spin–lattice relaxation times in the rotating frame is displayed in *Figure 9* for the CHOH–CH_2–O and CH_2–N carbons of the HMDA and HMDA/AP19 systems. At room temperature, the $T_{1\rho}(^{13}C)$ values are higher for the antiplasticized network than for the pure matrix. In the pure system, the $T_{1\rho}(^{13}C)$ values increase with temperature in the temperature range considered. On the contrary, in the HMDA/AP19 system, the $T_{1\rho}(^{13}C)$ values exhibit a decrease on increasing temperature above 60°C for both the CHOH–CH_2–O and CH_2–N groups. Since the above $t_{1/2}$ measurements have revealed the existence of motions in the tens of kHz region, the $T_{1\rho}(^{13}C)$ can be considered as originating mainly from spin–lattice processes. The $T_{1\rho}(^{13}C)$ spin–lattice relaxation time undergoes a minimum when the frequency of local motions is of the order of the intensity, expressed in frequency units, of the radio frequency field applied to the protons, i.e. 64 kHz. Therefore, the behaviour of the CHOH–CH_2–O and CH_2–N groups in the pure resin is typical of carbons undergoing motions with frequencies of the order of 64 kHz at room temperature whereas, in the HMDA/AP19 system, it corresponds to motions with frequencies slightly smaller than 64 kHz at 80°C. Therefore, both the $T_{1\rho}(^{13}C)$ and $t_{1/2}$ determinations indicate that the motions of the hydroxypropylether units are slowed down in presence of the antiplasticizer.

Local motions of the aromatic units. Results of $(t_{1/2})_0/t_{1/2}$ determinations performed as a function of temperature for the protonated aromatic carbons of the HMDA, HMDA/AP10 and HMDA/AP19 systems are shown in *Figure 10*. The pure and HMDA/AP10 systems exhibit quite similar behaviour. In the HMDA/AP19 resin, the onset of mobility of the aromatic carbons occurs at a higher temperature than in the pure matrix. This last result is very similar to that observed for the CHOH–CH_2–O units. In agreement with conclusions derived from the previous study of the HMDA system[1], it indicates a possible correlation between the motions of the aliphatic units and the ring flips.

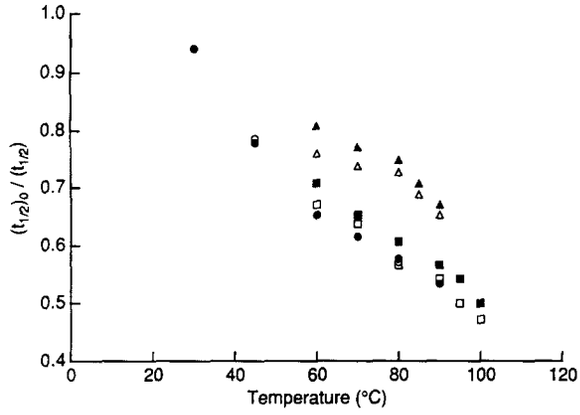

Figure 10 Temperature dependence of the $(t_{1/2})_0/t_{1/2}$ ratios, measured for the two protonated aromatic carbons of the HMDA (●,○), HMDA/AP10 (■,□) and HMDA/AP19 (▲,△) networks

Local dynamics of the antiplasticizer in the network. The inversion recovery cross-polarization pulse sequence (IRCP)[17] has been used for spectral editing[24]. Since, in this experiment, the contact time necessary to reach a zero magnetization depends on the dipolar coupling strength, this pulse sequence can also be considered as a useful tool for discriminating between overlapping peaks corresponding to carbons with different dynamics. Preliminary experiments performed on the HMDA system plasticized with dibutylphthalate have shown that the IRCP experiment can probe the local motions of the additive. The ^{13}C n.m.r. spectrum of the HMDA/AP19 sample at 80°C was obtained by using the IRCP pulse sequence and different cross-polarization times. As an example, the spectrum corresponding to a cross-polarization time of 40 μs is displayed in *Figure 11*. In the region of the hydroxypropylether carbons, the lines are close to cancellation. Their lineshape is similar to that observed in the classical CP experiment (*Figure 7*). No line specific of the EPPHAA molecule can be distinguished. The same result was obtained whatever the cross-polarization time, indicating that, within the sensitivity of the experiment, the hydroxypropylether sequences of the antiplasticizer and the matrix share similar local dynamics. Identical conclusions were derived from the behaviour of the resonances of the protonated aromatic carbons.

CONCLUSIONS

The different n.m.r. experiments reported above lead to an unambiguous characterization of the motional behaviour of each chemical group in the considered systems. In the present study, it thus clearly appears that the hydroxypropylether sequences and nitrogen crosslinks of the matrix are less mobile in the antiplasticized samples than in the pure networks. The phenyl ring flips are also slowed down.

With respect to the very local motional motions investigated by n.m.r., the dynamic mechanical analysis provides an interesting means for studying modes with a larger spatial extent. As shown by results obtained from this technique, the antiplasticizer acts mainly on the cooperative motions implying several repeat units. The disappearance of the cooperative motions in the antiplasticized densely crosslinked networks can be clearly related to the strong reduction in the crosslink mobility observed in the n.m.r. experiments. The n.m.r. experiments have also shown that the hydroxypropylether moieties are only slightly slowed

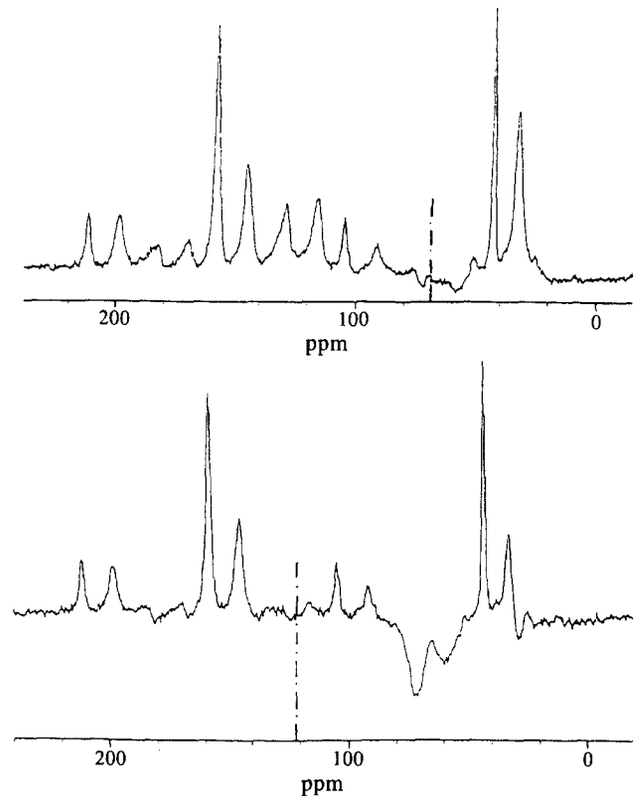

Figure 11 75 MHz High-resolution solid-state ^{13}C n.m.r. spectra of the HMDA/AP19 network obtained at 80°C by using the IRCP pulse sequence (top spectrum, contact time = 40 μs; bottom spectrum, contact time = 70 μs)

down. However, if the mobility of one hydroxypropylether unit is blocked by its interaction with an antiplasticizer molecule, the probability for cooperative motions to occur in its vicinity decreases dramatically, whereas the overall probability for isolated motions is just slightly diminished.

According to this description, a crude estimate of the number of hydroxypropylether units involved in the cooperative motions can be evaluated. Assuming a random distribution of the antiplasticizers in the vicinity of the hydroxypropylether moieties, there is one antiplasticizer molecule per three hydroxypropylether units in the HMDA/AP19 sample. Therefore, cooperative motions involving more than three units are unlikely to occur and the J'' peak of HMDA/AP19 should refer to motions involving no more than three units (*Figure 12*). Similarly, in the HMDA/AP10 system, there is one antiplasticizer molecule per six hydroxypropylether units and the processes responsible for the J'' peak cannot involve more than six units. As a consequence, the difference $J_{HMDA/AP19}'' - J_{HMDA/AP10}''$ corresponds to motions involving from three to six units (*Figure 12*). Finally, the $J_{HMDA/AP10}'' - J_{HMDA}''$ difference refers to cooperative motions with a longer spatial scale. The present estimate of the number of units involved in the cooperative motions is in very good agreement with the conclusions derived in our previous paper[1] from comparison of the compliances of the densely crosslinked HMDA network and of its loosely crosslinked homologue with pendant monoamine residues.

To get a deeper insight into the mechanism of antiplasticization, it is interesting to compare the above analysis with the conclusions reached by Spiess *et al.*[7] and Jones *et al.*[9] for antiplasticized polycarbonate. For polycarbonate, it is now recognized that the aromatic ring motions are responsible for the secondary transition through

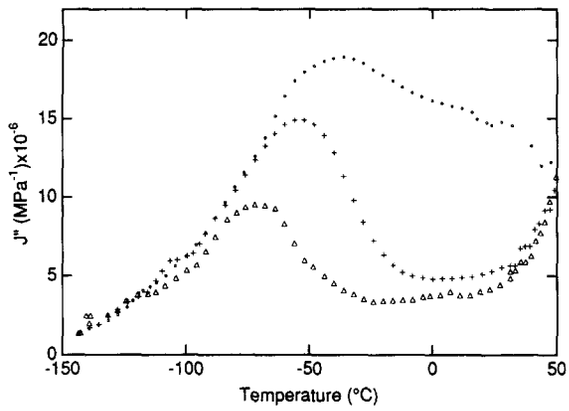

Figure 12 Schematic decomposition of the β transition of the HMDA network into motions involving: (from left to right) less than three crosslinks, between three and six crosslinks, and more than six crosslinks

a coupling with the chain backbone. The antiplasticization results in the slowing down of the ring flip rate, described in terms of Ngai formalism[25] as an enhancement of the dynamic coupling between the antiplasticizer and the polymer matrix. In this respect, the results reported in the present paper also indicate that the interactions between the EPPHAA molecules and the hydroxypropylether moiety of the network induce some dynamic coupling. This conclusion is supported by the n.m.r. analysis of the EPPHAA behaviour in the matrix, which has not revealed any difference between the mobilities of the polymer and the additive. A direct consequence is that the two components should share some rather strong interactions.

REFERENCES

1. Heux, L., Halary, J.L., Lauprêtre, F. and Monnerie, L., *Polymer*, 1997, **38**, 1767.
2. Shi, J. F., Inglefield, P. T., Jones, A. A. and Meadows, M. D., *Macromolecules*, 1996, **29**, 605.
3. Jackson, W. J. Jr. and Caldwell, J. R., *J. Appl. Polym. Sci.*, 1967, **11**, 211.
4. Hata, N., Yamauchi, R. and Kumanotani, J., *J. Appl. Polym. Sci.*, 1973, **17**, 2173.
5. Hata, N. and Kumanotani, J., *J. Appl. Polym. Sci.*, 1977, **21**, 1257.
6. Daly, J., Britten, A. and Garton, A., *J. Appl. Polym. Sci.*, 1984, **29**, 1403.
7. Wehrle, M., Hellmann, G. P. and Spiess, H. W., *Colloid Polym. Sci.*, 1987, **265**, 815.
8. Roy, A. K., Ingelfield, P. T., Shibata, J. H. and Jones, A. A., *Macromolecules*, 1987, **13**, 1127.
9. Jones, A. A., Ingelfield, P. T., Liu, Y., Roy, A. K. and Cauley, B. J., *J. Non-Cryst. Solids*, 1991, **131-133**, 556.
10. Khozin, V. G., Farrakhov, A. G. and Voskresenskii, V. A., *Polym. Sci. USRR*, 1979, **21**, 1938.
11. Khozin, V. G., Polyanskii, A. A., Budnik, Y. M. and Voskresenskii, V. A., *Polym. Sci. USRR*, 1982, **24**, 2646.
12. Garton, A., McLean, P. D., Stevenson, W. T. K., Clark, J. N. and Daly, J. H., *Polym. Eng. Sci.*, 1987, **27**, 1620–1626.
13. Merritt, M. E., Heux, L., Halary, J. L. and Schaefer, J., *Macromolecules*, in press.
14. Bauchière, D., Thèse, Université P. et M. Curie, Paris 1995.
15. Starkweather, H. W. J., *Macromolecules*, 1981, **14**, 1277.
16. Schaefer, J., Stejskal, E. O. and Buchdahl, R., *Macromolecules*, 1977, **10**, 384.
17. Cory, D. G., *Chem. Phys. Lett.*, 1988, **152**, 431.
18. Schaefer, J., Stejskal, E. O., Steger, T. R., Sefcik, M. D. and McKay, R. A., *Macromolecules*, 1980, **13**, 1121.
19. Herzfeld, J. and Berger, A. E., *J. Chem. Phys.*, 1980, **73**, 6023.
20. Ferry, J. D., *Viscoelastic Properties of Polymers*. John Wiley & Sons, New York, 1980.
21. Gérard, J. F., Galy, J., Pascault, J. P., Cukierman, S. and Halary, J. L., *Polym. Eng. Sci.*, 1991, **31**, 615.
22. Lauprêtre, F., Eustache, R. P. and Monnerie, L., *Polymer*, 1995, **36**, 267.
23. Lauprêtre, F., Monnerie, L. and Virlet, J., *Macromolecules*, 1984, **17**, 1397.
24. Wu, X. and Zilm, K. W., *J. Magn. Res.*, 1992, **102**, 205.
25. Ngai, K. L., Rendell, R. W., Yee, A. F. and Plazek, D. J., *Macromolecules*, 1991, **24**, 61.